Spectral composition and quanta-to-energy ratio of diffuse photosynthetically active radiation under diverse cloud conditions

Dennis G. Dye

Ecosystem Change Research Program, Frontier Research System for Global Change, Yokohama Institute for Earth Sciences, Japan Agency for Marine-Earth Science and Technology, Yokohama, Japan

Received 16 October 2003; revised 5 March 2004; accepted 23 March 2004; published 25 May 2004.

[1] Accurate and detailed modeling of vegetation photosynthesis and ecosystem-atmosphere CO_2 exchange, particularly for forests, requires data on the diffuse and global fluxes of photosynthetically active radiation (PAR) (400–700 nm). Such ecosystem process models typically employ PAR data in quantum units (photosynthetic photon flux density, Q_p, μmol m^{-2} s^{-1}), although PAR is often reported in energy units (irradiance, R_p, W m^{-2}). Reliable conversion of diffuse PAR data from energy units ($R_{p,d}$, W m^{-2}) to quantum units ($Q_{p,d}$, μmol m^{-2} s^{-1}) requires knowledge of how the conversion factor $\beta^*_{p,d}$ (quanta-to-energy ratio for diffuse PAR at an arbitrary timescale, μmol J^{-1}) varies across a broad range of sky conditions that includes variations in cloudiness, including broken clouds. This study employs spectral measurements of the diffuse irradiance of PAR to examine the influence of a diverse range of observed sky conditions on the spectral composition of $R_{p,d}$ and the value of $\beta^*_{p,d}$ at 1-minute and daily timescales. The results indicate that the enhanced contribution of green-to-red (550–700 nm) radiation to the spectral composition of $R_{p,d}$, induced by atmospheric scattering and diffuse reflectance by clouds, causes $\beta^*_{p,d}$ at the daily timescale ($\beta'_{p,d}$) to increase nonlinearly by up to 7% relative to clean, cloudless sky conditions. The relation is explained well (R = 0.98) by the equation $\beta'_{p,d} = (4.5886 \times f'_{p,d})/(0.010773 + f'_{p,d})$, where $f'_{p,d}$ is equal to the diffuse fraction of the daily total irradiation of global PAR. These results may be useful for conversion of diffuse PAR data between energy and quantum units for environments where clouds are the dominant agent of atmospheric scattering. The observed quanta-to-energy ratio for global PAR at the daily timescale ($\beta'_{p,g}$), while not strictly constant, is relatively insensitive to atmospheric scattering, and a representative value of 4.56 μmol J^{-1} may be employed for a wide range of cloud conditions with little or no error. *INDEX TERMS:* 0315 Atmospheric Composition and Structure: Biosphere/atmosphere interactions; 1615 Global Change: Biogeochemical processes (4805); 3359 Meteorology and Atmospheric Dynamics: Radiative processes; 1851 Hydrology: Plant ecology; *KEYWORDS:* photosynthetically active radiation, PAR

Citation: Dye, D. G. (2004), Spectral composition and quanta-to-energy ratio of diffuse photosynthetically active radiation under diverse cloud conditions, *J. Geophys. Res.*, *109*, D10203, doi:10.1029/2003JD004251.

1. Introduction

[2] Photosynthetically active radiation (PAR, 400–700 nm) from the sun provides the energy that supports photosynthesis and primary production by green plants. PAR is therefore a key variable in process-based models of terrestrial photosynthesis and ecosystem-atmosphere CO_2 exchange. Although terrestrial ecosystem process models frequently account for global PAR (the PAR received from all directions in the sky hemisphere), a growing body of research indicates that accurate simulation of vegetation photosynthesis at daily and subdaily timescales, particularly for forest canopies, requires separate treatment of the directional components of global PAR: the diffuse and direct beam PAR [*Allen et al.*, 1974; *McCartney*, 1978; *Healey et al.*, 1998; *Roderick et al.*, 2001; *Gu et al.*, 2002; *Farquhar and Roderick*, 2003; *Medlyn et al.*, 2003].

[3] In satisfying this data requirement, at least two major problems may be confronted. First, measurement data on diffuse and beam PAR are not commonly available [*Ross and Sulev*, 2000]. The PAR sensors at meteorological or ecological observation stations around the globe typically measure only global PAR. Although deployment of sensors with the additional capability of measuring diffuse PAR is steadily increasing, at this time data from such sensors remain comparatively rare. (In practice, measurements of only global and diffuse PAR are sufficient, since the direct beam component can be calculated as the difference of these two fluxes.) A practical solution to

0148-0227/04/2003JD004251

the paucity of measurement data is to estimate diffuse PAR with an empirical model, given measured or predicted values of either global PAR or global, broadband solar radiation. Although the necessity of this approach may be justifiable in the absence of a reliable measurement-based PAR data source, such empirical estimates of diffuse PAR may include bias or inaccuracy that hinder progress toward deeper understanding and improved predictability of radiation-canopy-photosynthesis relations.

[4] The second problem concerns the incompatibility between the physical units in which PAR is often measured or reported, and the units that are appropriate for process-based modeling of photosynthesis. Photosynthesis is a photochemical process that depends more on the number of photons absorbed than on the energy content of those photons [*Hall and Rao*, 1994]. Thus models that simulate the photosynthetic response of leaves or canopies to PAR typically require PAR data in quantum units (photosynthetic photon flux density, Q_p, μmol m^{-2} s^{-1}). On the other hand, PAR data (or broadband solar radiation data, from which PAR may be estimated) are often reported in energy units (irradiance, R_p or R_s, W m^{-2}, where the subscripts p and s indicate PAR and broadband solar radiation, respectively) [*Frouin et al.*, 1989; *Bishop and Rossow*, 1991; *Pinker and Laszlo*, 1992; *Dye and Shibasaki*, 1995; *Data Assimilation Office* (*DAO*), 2003]. This unit incompatibility is usually resolved by application of a conversion factor $\beta^*_{p,n}$ (quanta-to-energy ratio, μmol J^{-1}), where the subscript variable n refers to global (g), diffuse (d), or direct beam (b) radiation, and the asterisk indicates an arbitrary or indeterminate timescale.

[5] The value of $\beta^*_{p,n}$ is fundamentally determined by the spectral composition of the incident global, diffuse or beam irradiance in the 400–700 nm wave band. The spectral composition is determined by the selective (or non-selective) scattering of beam PAR by the various atmospheric components (molecular gases, aerosols, and clouds) and their distribution across the sky hemisphere. The irradiance spectrum of global PAR on an unobstructed, horizontal patch at the surface is determined by the combination of the radiance spectra of all light sources (the solar disk, broken or uniform clouds, blue-sky in cloud gaps, turbid sky in cloud gaps, etc.) that illuminate the patch (*Endler*, 1993). The global PAR spectrum is equal to the sum of the radiant spectra of the component light sources, weighted by the solid angles that they subtend. The diffuse PAR spectrum is equal to the difference of this sum and the contribution from the direct beam PAR.

[6] In the case of global PAR, several studies indicate that $\beta^*_{p,g}$ is virtually insensitive to changes in both cloudiness [*Zhou and Xiang*, 1992] and fine mode aerosols [*McCartney*, 1978; *Jacovides et al.*, 1997]. Results from these studies and data reported by *McCree* [1972] suggest that a constant value of $\beta^*_{p,g}$ = 4.57 μmol J^{-1} could be adopted for general application with little or no error. In the case of diffuse PAR, $\beta^*_{p,d}$ is markedly sensitive to sky conditions. Several studies have examined the spectral distribution of $R_{d,p}$ or $R_{d,s}$, and/or the value of $\beta^*_{p,d}$ for cloudless skies with and without aerosols. An early analysis of the spectral composition of diffuse solar radiation ("skylight") by *Diermendjian and Sekera* [1954] shows that Rayleigh scattering by a clean, clear atmosphere causes the maximum spectral irradiance in the PAR region to shift toward longer wavelengths as the solar elevation angle (SEA) decreases (i.e., as relative air mass increases) and blue radiation becomes depleted. The result of this spectral shift is a relative decrease in diffuse irradiance at short blue wavelengths (~400–430 nm) and a relative increase in diffuse irradiance at green and red (~500–700 nm) wavelengths [*Gates*, 1966].

[7] Other researchers have examined the effects of scattering by aerosols (turbidity) on the spectral distribution of solar irradiance and PAR. The aerosol optical depth of fine mode (submicron) aerosols in the PAR spectral region, and likewise their scattering of PAR, has a strong spectral dependence [*Salby*, 1996]. For a fixed SEA value, the effect of increased turbidity associated with fine mode aerosols on the spectral composition of PAR is qualitatively similar to the effect of decreased SEA under clear skies, i.e., the spectral distribution shifts toward longer (red) wavelengths [*McCree*, 1976; *McCartney*, 1978; *Brine and Iqbal*, 1983; *Jacovides et al.*, 1997]. *McCartney* [1978] and *Jacovides et al.* [1997] show that for moderate and high solar elevation angles at a rural and urban site, respectively, $\beta^*_{p,d}$ is 4.22–4.27 μmol J^{-1} under a clean, cloudless atmosphere, but increases to 4.34–4.43 μmol J^{-1} under a cloudless but highly turbid atmosphere. In these studies, highly turbid conditions are associated with an aerosol optical depth of 0.43–0.85 (at 500 nm) for the urban site [*Jacovides et al.*, 1997], and 0.5 (visible region) for the rural site [*McCartney*, 1978]. Neither *McCartney* [1978] nor *Jacovides et al.* [1997] report particle size distributions corresponding to these aerosol optical depth values, however aerosols in urban and rural environments generally consist of predominately fine mode particles [*Hinds*, 1999].

[8] The reported effects of aerosol-induced scattering on $\beta^*_{p,d}$ do not apply to cloudy conditions because scattering in the PAR spectral region by clouds, in contrast to fine mode aerosols, is essentially wavelength independent [*Salby*, 1996]. Clouds are often the predominant agent of scattering or diffuse reflection of PAR in the atmosphere, therefore information on how they affect $\beta^*_{p,d}$ can be essential for reliable conversion of diffuse PAR data from energy units to quantum units and *vice versa*. A review of the literature revealed no prior, published study of how $\beta^*_{p,d}$ varies across a broad range of sky conditions that includes variations in cloudiness, including broken clouds. The present study addresses this information gap. I employ field measurements of spectral and broadband irradiance of PAR to quantify the combined effects of atmospheric scattering and diffuse reflectance of PAR associated with a diverse set of sky conditions on the spectral composition of diffuse PAR and on the value of $\beta^*_{p,d}$ at 1-minute and daily timescales ($\beta_{p,d}$ and $\beta'_{p,d}$, respectively). For comparison, I also examine the effects on the spectral composition of global PAR and $\beta^*_{p,g}$ at 1-minute and daily timescales ($\beta_{p,g}$ and $\beta'_{p,g}$, respectively). I show that the predominant source of atmospheric scattering of PAR at the study site in Oklahoma, USA is typically clouds rather than aerosols. Empirical equations are presented that may be applied to convert daily diffuse and global PAR data between energy

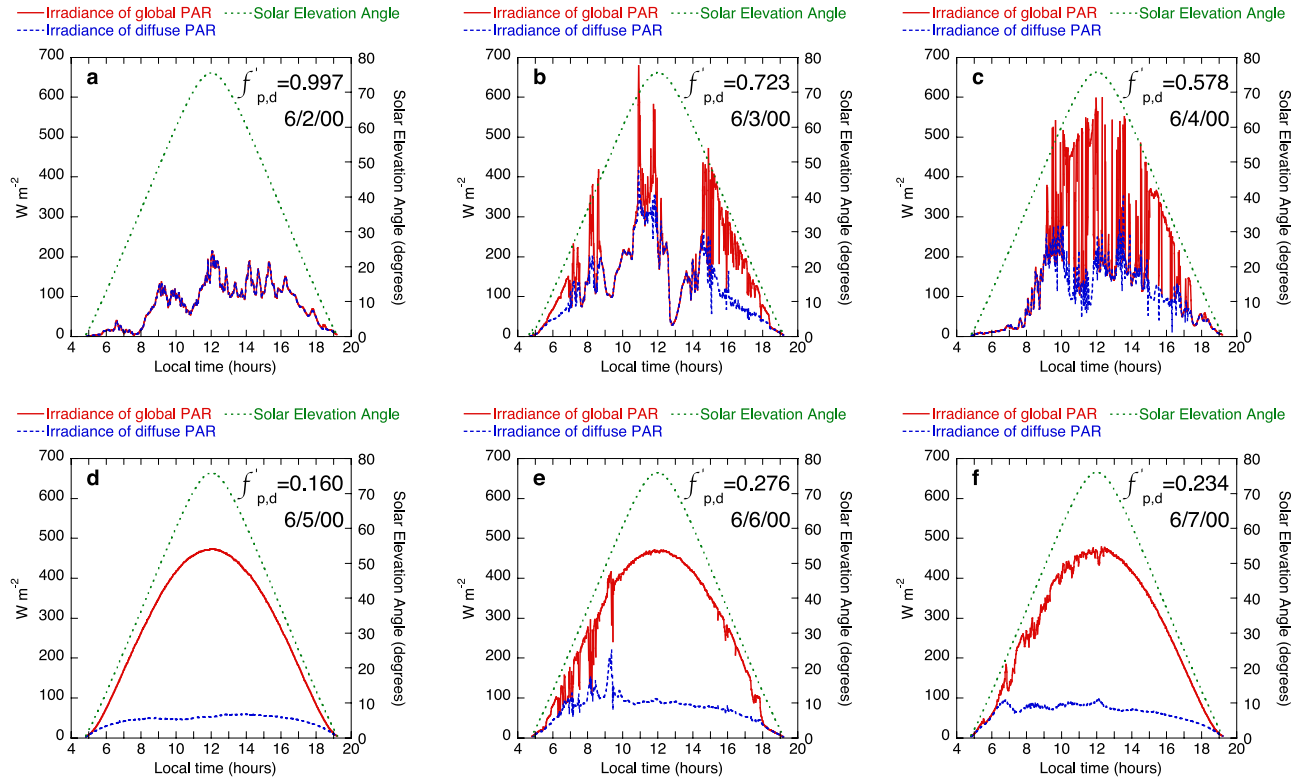

Figure 1. (a–f) Diurnal time series measurements of 1-min average diffuse and global irradiance of photosynthetically active radiation (PAR) and coincident variation in solar elevation angle for six consecutive days (2–7 June 2000) with contrasting sky conditions. The variable $f'_{p,d}$ is equal to the diffuse fraction of the daily total global irradiation of PAR. The data were collected in Oklahoma at the Southern Great Plains (SGP) site of the Atmospheric Radiation Measurement (ARM) program.

and quantum units for locations where clouds are the predominant causal agents of diffuse irradiance at the surface.

2. Data and Methods

2.1. Time Series Measurements of the Spectral Irradiance of Photosynthetically Active Radiation (PAR)

[9] The spectral composition of diffuse PAR and the values of $\beta_{p,d}$ and $\beta'_{p,d}$ are determined by analysis of a time series of spectral irradiance measurements collected with the Rotating Shadowband Spectroradiometer (RSS) at the Southern Great Plains (SGP) site of the Atmospheric Radiation Measurement (ARM) Program in Oklahoma, USA (latitude 36.606°N, longitude 97.485°W) [*Harrison et al.*, 1999]. The RSS measurements include global-horizontal and diffuse-horizontal spectral irradiance ($R_{i,g}$, and $R_{i,d}$, respectively, W m^{-2} nm^{-1}) at 1016 spectral channels i centered on wavelengths $\lambda(i)$ between 360 and 1100 nm. These irradiance variables are measured with a single charged-coupled device (CCD) spectrograph. The unique strength of the RSS instrument design is its capability to avoid errors that may otherwise result from inconsistencies in sensor calibration, bandpass sensitivity, or sensor drift when separate instruments are used for measurement of diffuse and global (or diffuse and beam) irradiance. In the present study, I restrict the analysis to the 573 spectral channels (i = 190, 762) that cover the 400–700 nm region, for which $\lambda(190) = 400.1755$ nm and $\lambda(762) = 699.8263$ nm.

[10] The RSS data set employed in this study contains 1-minute average values of $R_{i,g}$ and $R_{i,d}$ collected for the 153 consecutive days covering the period from March 1, 2000 to July 31, 2000. Fifty days with incomplete diurnal time series were rejected, and data for the remaining 103 days were retained for analysis. The final data set consists of ~47.7 million individual spectral measurements corresponding to 83,186 discrete, 1-minute measurement intervals. The minimum and maximum observed solar elevation angles are 0.4 and 76.8 degrees, respectively. The diurnal time series of the spectrally integrated (broadband) irradiance of PAR for a sample set of six consecutive days (June 2–7, 2000) with contrasting sky conditions are displayed in Figure 1. High frequency variability apparent in the diurnal time series is indicative of broken clouds (Figures 1b, 1c, and 1e). The complete time series of the daily total irradiation of PAR is displayed in Figure 2a. The observed variation in the diffuse fraction of the daily global irradiation of PAR ($f'_{p,d}$) (Figure 2b) indicates that the data set represents a diverse set of daily sky conditions, ranging from clear (e.g., Figure 1d) to 100% overcast (e.g., Figure 1a).

2.2. Sources of Diffuse PAR at the Study Site

[11] The primary cause of diffuse PAR at the Earth's surface is scattering by the molecular atmosphere and, when present, aerosols and/or clouds. Apart from variation in solar elevation angle (SEA), variation in the amount and properties of aerosols and/or clouds is the major source of spatial and temporal variation in diffuse PAR. Because the scatter-

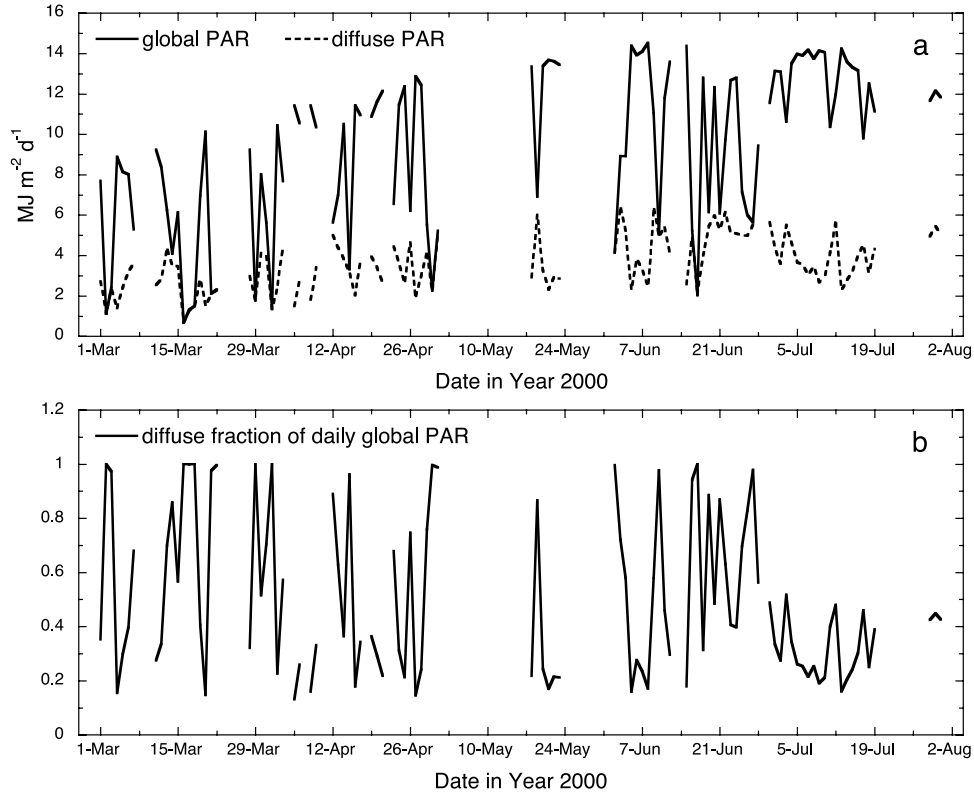

Figure 2. Time series of (a) daily diffuse and global irradiation of PAR and (b) corresponding values of the diffuse fraction of the daily global irradiation of PAR. These daily data were calculated from the measured spectral irradiation of diffuse and global PAR for 1-min intervals.

ing of PAR by fine mode aerosols and by clouds differ in their spectral behavior, correct interpretation of the results of the present study requires attribution of the observed diffuse PAR to a predominant scattering medium. Several available data sources suggest that clouds, rather than aerosols, are typically the predominant scattering medium at the SGP site.

[12] *Iziomon and Lohmann* [2003] report that fine mode aerosols dominate the aerosol-related scattering at the SGP site for all hours and all seasons. Measurement data reported by *Michalsky et al.* [2001] for years 1993 to 2000 indicate the daily average aerosol optical depth at 500 nm typically varies between an annual minimum of ~0.06–0.8 in winter and an annual maximum of ~0.15–0.19 in summer, although values as low as ~0.02 and as high as ~0.40 are observed on individual days. The seasonal median of the Angstrom exponent (single scattering albedo) as determined from measurements collected in years 1997 through 2001 are 2.17 (0.95) for spring (March through May) and 2.15 (0.93) for summer (June through August) [*Iziomon and Lohmann*, 2003].

[13] On the basis of model results reported by *Eck et al.* [2003] for a cloudless sky and SEA = 60°, aerosol conditions at the SGP site for a typical summer day (assuming an aerosol optical depth at 500 nm of 0.19 and single scattering albedo of 0.95, as supported by *Iziomon and Lohmann* [2003]) would yield a diffuse fraction of global PAR at an instantaneous time-scale ($f_{p,d}$) of ~0.20, or ~0.14 under a nominally clean atmosphere (with an aerosol optical depth of 0.10). In the present study, the mean (standard deviation) $f_{p,d}$ observed at SGP at the 1-minute timescale under similar solar elevation conditions ($59° < SEA < 61°$) is 0.45 (0.36) for April–July (n = 2068), and 0.50 (0.36) for June–July (n = 1026). Thus at this near-instantaneous timescale and for this sample range of SEA, the large differences between $f_{p,d}$ for the cloudless case with typical summer aerosols (0.30 for June–July) and the $f_{p,d}$ observed in the present study are attributable to scattering agents other than fine mode aerosols. This comparison, together with *Iziomon and Lohmann*'s [2003] observation that fine mode aerosols consistently dominate the aerosol-related scattering at the SGP site, suggests that cloudiness, as opposed to aerosols of any particle size, are typically the dominant source of diffuse irradiance at the site. This suggestion is reinforced by cloud fraction (CF) data, which show that the time-averaged value of CF at the SGP site is substantial throughout the study period (0.34–0.62 at the monthly timescale) (Table 1). Monthly mean CF values

Table 1. CF Statistics for the SGP Site During the Study Period, Calculated From Observation Data Reported by *Rutan et al.* [2001][a]

Month in 2000	No. of Observation Days (%)	Mean CF, (standard deviation)
March	31 (100.0)	0.62 (0.38)
April	22 (73.3)	0.46 (0.35)
May	21 (67.7)	0.42 (0.37)
June	30 (100.0)	0.60 (0.31)
July	31 (100.0)	0.34 (0.26)
March–July	135 (88.2)	0.49 (0.35)

[a]CF, cloud fraction, dimensionless; SGP, Southern Great Plains; No., number.

(Table 1) are calculated from values of daily mean CF obtained from an observation data set prepared by the CERES/ARM Validation (CAVE) Experiment [*Rutan et al.*, 2001].

2.3. Quanta-to-Energy Ratios for PAR

[14] The quanta-to-energy ratios for diffuse and global PAR are quantified at two timescales: 1-minute ($\beta_{p,n}$) and daily ($\beta'_{p,n}$). Both $\beta_{p,n}$ and $\beta'_{p,n}$ have units of μmol J^{-1} (or equivalently, mol MJ^{-1}). At the 1-minute timescale,

$$\beta_{p,n} = \frac{Q'_{p,n}}{R'_{p,n}} \tag{1}$$

where $R'_{p,n}$ is the irradiation (J m^{-2}) for a single 60-second measurement interval, and $Q'_{p,n}$ is the corresponding photon exposure (μmol m^{-2}). For the daily timescale, $\beta'_{p,n}$ is similarly calculated with the daily total irradiation ($R''_{p,n}$, MJ m^{-2}), and the corresponding daily total photon exposure ($Q''_{p,n}$, mol m^{-2}). The steps taken to calculate these energy and photon variables with the spectral irradiance data ($R_{i,d}$ and $R_{i,g}$) from the RSS instrument are described in Appendix A.

2.4. Spectral Composition of Diffuse PAR

[15] To evaluate the effect of atmospheric scattering and diffuse reflection on the spectral composition of diffuse PAR, I qualitatively examine the observed variation in the spectral distribution of diffuse PAR energy and quanta. The corresponding spectral distributions for global PAR are also examined. The distribution of PAR between the 400–550 nm and 550–700 nm spectral regions is quantitatively evaluated on the basis of a dimensionless index, referred to here as the Normalized Difference PAR Spectral Index (NDPSI). The NDPSI at the daily timescale is calculated as

$$\mathrm{NDPSI}'_{E,n} = \frac{R''_{pir,n} - R''_{puv,n}}{R''_{pir,n} + R''_{puv,n}} \tag{2}$$

and

$$\mathrm{NDPSI}'_{Q,n} = \frac{Q''_{pir,n} - Q''_{puv,n}}{Q''_{pir,n} + Q''_{puv,n}} \tag{3}$$

where the subscripts E and Q indicate an energy basis and quantum basis, respectively. The subscripts puv and pir refer to the 400–550 nm and 550–700 nm wave bands, respectively. The subscript variable n is either d (diffuse) or g (global). The maximum theoretical range is $-1.0 \leq \mathrm{NDPSI} \leq 1.0$, where −1.0 (+1.0) indicates that 100% of the PAR energy or quanta are from radiation in the 400–550 nm (550–700 nm) wave band, however in reality these limits will never be reached. For NDPSI = 0.0, the spectral distribution is balanced (equal amounts of PAR energy or quanta are from radiation with wavelengths longer than, and shorter than, 550 nm). A negative (positive) deviation in NDPSI from zero indicates a bias in the spectral distribution of PAR energy or quanta toward the 0.40–0.55 μm (0.55–0.70 μm) region. The absolute value of NDPSI indicates the magnitude of this bias, in physical terms, as a fraction of the measured broadband (0.40–0.70 μm) PAR. Although the spectral division at the central PAR wavelength of 550 nm is arbitrary, when the plotted against a corresponding value of $f'_{p,d}$, the NDPSI provides a convenient, intuitive measure of change in the relative spectral distribution of energy or photons within the PAR wave band.

2.5. Atmospheric Scattering of PAR Under Diverse Sky Conditions

[16] The relative magnitude of atmospheric scattering or diffuse reflection of PAR is quantified as a dimensionless ratio equal to the diffuse fraction of the global irradiance of PAR ($f_{p,d}$). At the 1-minute timescale, the diffuse fraction is calculated as

$$f_{p,d} = \frac{R'_{p,d}}{R'_{p,g}} \tag{4}$$

The diffuse fraction of global PAR at the daily timescale ($f'_{p,d}$) is similarly calculated with $R''_{p,d}$ and $R''_{p,g}$.

[17] In the present analysis, scattering by the molecular atmosphere, aerosols, and clouds and diffuse reflection by clouds are considered as a single, bulk phenomenon that produces diffuse irradiance at the surface, and their respective contributions are not quantitatively differentiated. One shortcoming of this approach is that it does not account for potential differences in the spectral absorption and scattering characteristics of aerosols and clouds, which could produce different spectral compositions of diffuse PAR for a common value of $f_{p,d}$. Apart from the sun angle-dependent effects of Rayleigh scattering of PAR by a clean, cloudless atmosphere, clouds (and their associated physical, spatial and geometric attributes) are the predominant source of the large variation in $f_{p,d}$ (∼0.10–1.0) observed at the SGP site (Figure 2b), as discussed above. Aerosols are assumed to be a secondary and less significant source of atmospheric scattering. The results presented here may therefore be most applicable to environments or conditions in which clouds are the major source of day-to-day variation in diffuse PAR.

[18] A second, potential shortcoming is that $f_{p,d}$ does not explicitly account for the spatial and geometric characteristics of clouds, which could be an additional source of variation in the spectral composition of diffuse PAR, and in $\beta_{p,d}$. A detailed, quantitative examination of this influence would require coincident information on the three-dimensional, hemispheric distribution of clouds and aerosols and the corresponding source geometry of the spectral radiance of PAR. Such an analysis is beyond the scope the present study.

[19] In the present study, I investigate the combined influence of atmospheric scattering and diffuse reflectance on the spectral composition of diffuse PAR at the daily scale by examining the relationship between $f'_{p,d}$ and corresponding measures of $\mathrm{NDPSI}'_{E,n}$ and $\mathrm{NDPSI}'_{Q,n}$ from Equations 2 and 3. I analyze the relation between atmospheric scattering and the quanta-to-energy ratios for PAR by examining the relations between $f_{p,d}$ and $\beta_{p,n}$ (1-minute scale), and between $f'_{p,d}$ and $\beta'_{p,n}$ (daily timescale).

3. Results and Discussion

3.1. Spectral Composition of Diffuse PAR Under Diverse Cloud Conditions

[20] Atmospheric scattering (including diffuse reflectance from clouds) induces a distinct shift in the spectral composition of daily diffuse PAR (Figures 3 and 3b). As $f'_{p,d}$

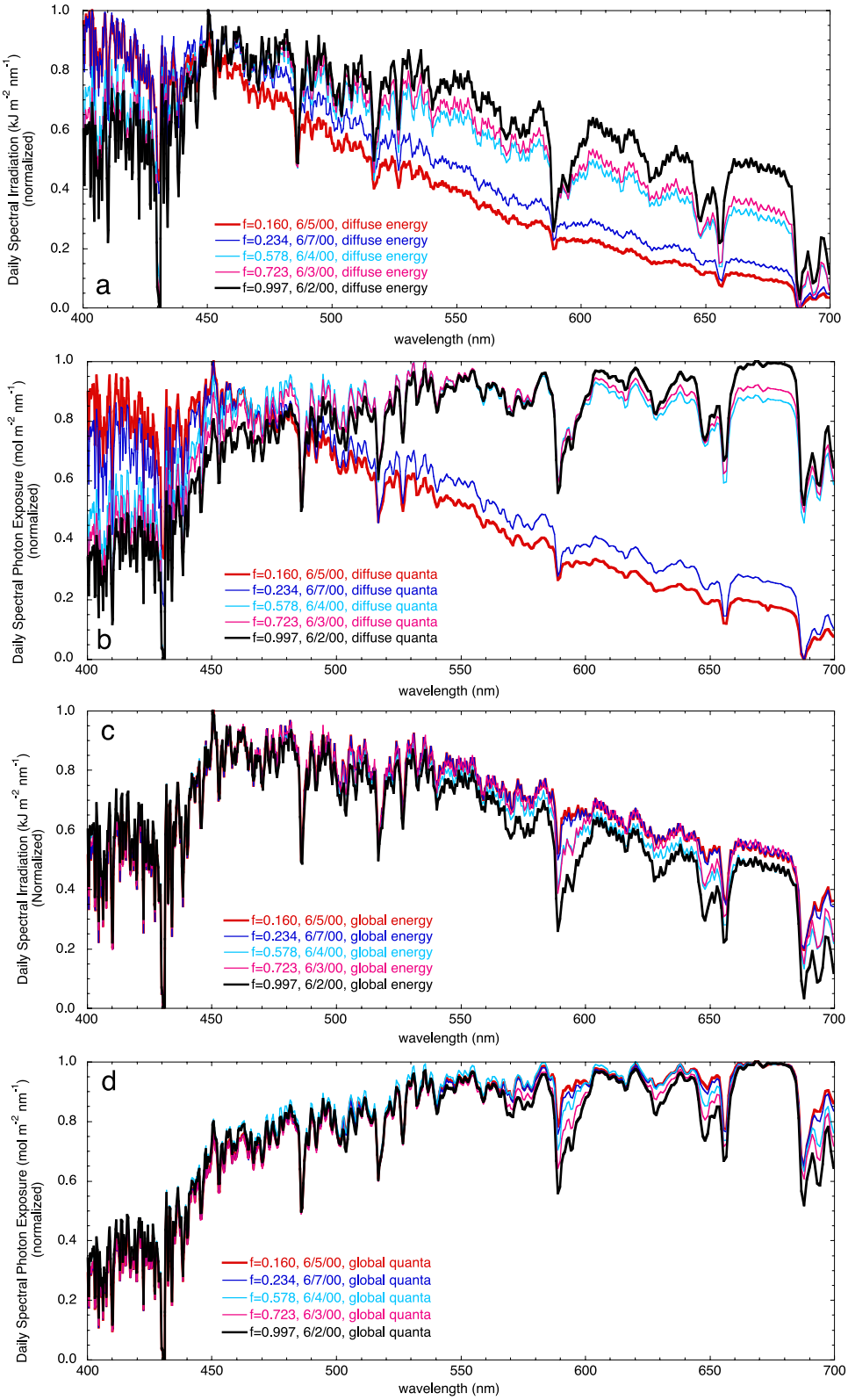

Figure 3. The spectral distribution of the normalized daily diffuse PAR in terms of (a) energy and (b) quanta, and the spectral distribution of normalized daily global PAR in terms of (c) energy and (d) quanta. For each data plot, values of spectral irradiation or photon exposure were normalized to the maximum range of these values observed among the individual days. The curves represent five consecutive days (2–6 June 2000) with diverse sky conditions as indicated by values of f (diffuse fraction of daily total global irradiation of PAR), where $f = f'_{p,d}$.

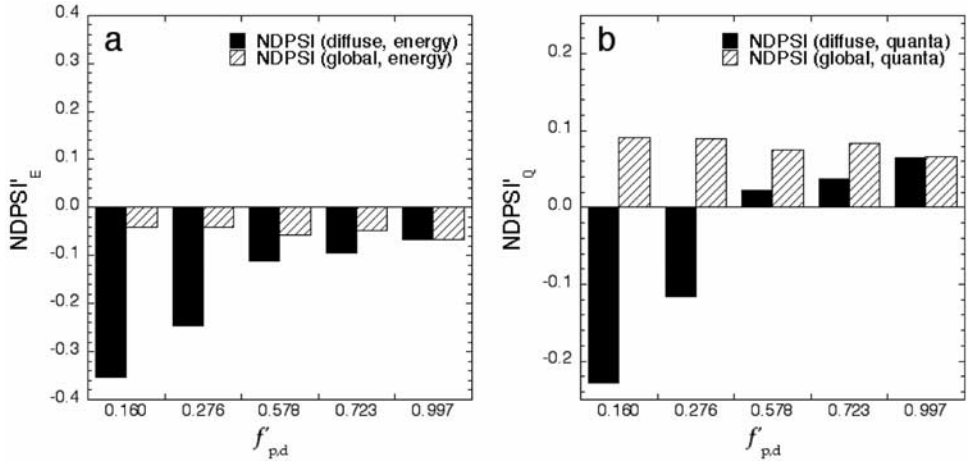

Figure 4. Values of the Normalized Difference PAR Spectral Index (NDPSI) for daily diffuse PAR (solid bars) and global PAR (hatched bars) in terms of (a) energy ($NDPSI'_E$]) and (b) quanta ($NDPSI'_Q$) for days with different magnitudes of atmospheric scattering as indicated by $f'_{p,d}$. Negative (positive) values indicate the relative magnitude of bias in the spectral distribution of PAR energy or quanta to the 0.40–0.55 μm (0.55–0.70 μm) region. These results are for 2–6 June 2000, and correspond to days depicted in Figures 1 and 3.

increases from a low value associated with clear sky conditions (~0.16) toward a near-maximum value associated with virtually 100% overcast conditions (~0.997), the relative proportion of energy received from short-wavelength blue radiation (e.g., 400–425 nm) declines, while relative proportion of energy from the longer wavelength green and red radiation (e.g., 500–700 nm) increases (Figure 3a). This pattern is accentuated when viewed in quantum terms (Figure 3b). The large changes in photon exposure at red (long) wavelengths relative to blue (short) wavelengths (Figure 3b) are attributable to the inverse relation between the wavelength of radiation and the energy of a single photon of that radiation as determined by quantum law (Equation A5).

[21] The transition of the spectral composition of diffuse PAR between the two extreme sky conditions (from cloudless to overcast, or from $f'_{p,d} \approx 0.16$ to $f'_{p,d} \approx 0.997$) is attributable to a shift in the predominant scattering regime from selective (Rayleigh) scattering by the molecular atmosphere to non-selective scattering by extensive cloud cover. Because Rayleigh scattering preferentially scatters short wavelength (blue) radiation, diffuse PAR under a cloudless sky exhibits the well known spectral peak in the blue region (Figures 3a and 3b). As cloudiness increases, the contribution from non-selective scattering to the diffuse PAR component increases, thereby increasing the relative proportion of radiation at green and red wavelengths (Figures 3a and 3b).

[22] As direct beam PAR traverses from the top of the atmosphere to the surface, atmospheric scattering redirects a portion of the radiation to the diffuse component of global PAR. Whereas the spectral composition of diffuse PAR varies according to the predominant scattering regime (molecular atmosphere, aerosols, and/or clouds), the spectral composition of global PAR (the combination of the direct beam and diffuse PAR components) is a conservative feature in the absence of significant, selective atmospheric absorption. Because atmospheric absorption of PAR is relatively low or negligible under typical conditions, PAR may be selectively and/or non-selectively scattered away from the direct beam without substantial change to the spectral properities of the global flux. This phenomenon is apparent in Figures 3c and 3d; in contrast to the diffuse PAR case, the spectral composition of daily global PAR is almost independent of $f'_{p,d}$. Analysis of the NDPSI (Figure 4) shows that an increase in $f'_{p,d}$ is associated with a relative increase in the allocation of energy and photons at green and red (550–700 nm) wavelengths to diffuse PAR, as indicated by the relatively large rise in NDPSI for the diffuse PAR case. In terms of energy (quanta), the NDPSI for global PAR is relatively constant near −0.04 to −0.06 (+0.06 to +0.09). This result indicates that the spectral distribution of global PAR energy (quanta) is relatively stable at the daily timescale for all observed cloud conditions, and consistently biased to the 400–550 nm (550–700 nm) region (Figure 4).

3.2. Effects of Atmospheric Scattering on the Quanta-to-Energy Ratio for PAR

3.2.1. One-minute Timescale

[23] Photons of short wavelength radiation are more energetic than photons of longer wavelength radiation, therefore the number of photons per unit of radiant energy increases as the wavelength of the radiation increases. Consequently, a scattering-induced shift in the spectral composition of diffuse PAR toward longer wavelengths (Figures 3 and 4) should generally cause $\beta_{p,d}$ to increase. Indeed, this general effect is apparent at the 1-minute timescale (Figure 5a). The relation between $f_{p,d}$ and $\beta_{p,d}$ (Figure 5a) exhibits an additional, complex dependence on SEA. For moderate and high values of SEA and for $f_{p,d} \lesssim 0.97$, the relation is distinctly non-linear, rising from ~4.23 μmol J^{-1} under clear conditions ($f_{p,d} \approx 0.10$) and approaching a saturating value of ~4.57 μmol J^{-1} at moderate levels of scattering ($f_{p,D} \approx 0.4 \sim 0.6$) (Figure 5a). In the case of global PAR (Figure 5b), a shallow, linear relation between $f_{p,d}$ and $\beta_{p,g}$ is apparent for SEA $\gtrsim$ 25 degrees.

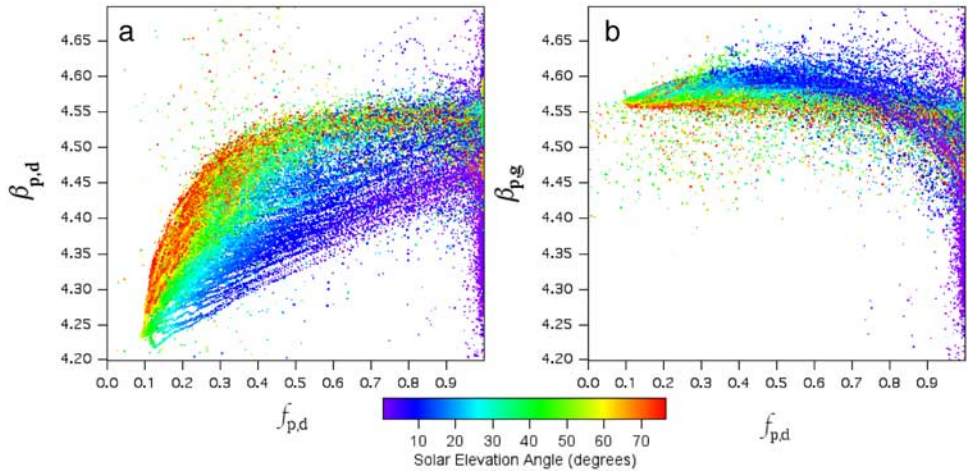

Figure 5. Relationship between the magnitude of atmospheric scattering (indicated by the diffuse fraction of the global irradiation of PAR, $f_{p,d}$) and the quanta-to-energy ratios (a) for diffuse irradiation of PAR ($\beta_{p,d}$) and (b) for global irradiation of PAR ($\beta_{p,g}$). The color scale indicates corresponding values of the solar elevation angle. These results represent the complete set of 83,186 1-min average measurements collected on 103 days in the period from 1 March to 31 July 2000.

Factors that are not well represented by $f_{p,d}$, such as the horizontal distribution and geometrical and optical properties of clouds and/or aerosols, may exert additional influence on the relationships apparent in Figures 5a and 5b.

[24] For extreme conditions in which PAR is essentially 100% diffuse ($0.97 \leq f_{p,d} \leq 1.0$), $\beta_{p,d}$ and $\beta_{p,g}$ become approximately equal and exhibit a broad range values ($\sim$4.23 to $\sim$4.68). The highest and lowest values (e.g., $\beta_{p,d} > 4.55$ and $\beta_{p,d} < 4.4$) are primarily associated with extremely low SEA (<10°). In contrast, moderate values ($4.4 < \beta_{p,d} < 4.55$) are associated with a broad range of SEA values. The observed scatter of $\beta_{p,d}$ and $\beta_{p,g}$ under 100% diffuse conditions may be attributable to mechanisms that vary with SEA and sky conditions. In general, any phenomenon that increases (decreases) the proportion of green-to-red wavelength irradiance relative to blue-to-green wavelength irradiance would cause $\beta_{p,d}$ and $\beta_{p,g}$ to decline (increase). Potential mechanisms include (1) wavelength-dependent absorption by ozone, aerosols, and water vapor and/or three-dimensional scattering effects by clouds when SEA approaches 0 degrees and the relative air mass becomes extremely high, and (2) wavelength-dependent absorption by cloud drops, water vapor and possibly aerosols under conditions of fog or 100% cloud cover with extremely high cloud optical thickness.

[25] Figure 6 compares the relation between $\beta_{p,d}$ and SEA for four classes of $f_{p,d}$ as determined in the present study and from data for Athens, Greece reported by *McCartney* [1978]. In the present study, differences in $f_{p,d}$ are attributable primarily to clouds, whereas in *McCartney*'s [1978] study, the differences in $f_{p,d}$ are caused primarily (or solely) by fine mode aerosols. For a fixed value of SEA, the relations between $f_{p,d}$ and $\beta_{p,d}$ for the two data sets are *qualitatively similar*: both show that an increase in $f_{p,d}$ is associated with an increase in $\beta_{p,d}$. In contrast, the relations between $f_{p,d}$ and $\beta_{p,d}$ are *quantitatively dissimilar*. For paired values of SEA and $f_{p,d}$, $\beta_{p,d}$ for a cloudy sky is consistently higher than $\beta_{p,d}$ for a turbid sky (disregarding *McCartney*'s [1978] single, anomalous value for SEA = 40 degrees and $0.232 < f_{p,d} < 0.245$). An additional, significant difference in the relationship between $f_{p,d}$ and $\beta_{p,d}$ for cloudy conditions (this study) and the relation for cloudless but turbid skies [*McCartney*, 1978] is apparent in Figure 6. For a fixed, narrow range of $f_{p,d}$ (displayed as blue, green or red in Figure 6), $\beta_{p,d}$ under cloudy skies *increases* with increasing SEA, whereas $\beta_{p,d}$ under turbid skies *decreases* with increasing SEA. These opposing relations may be

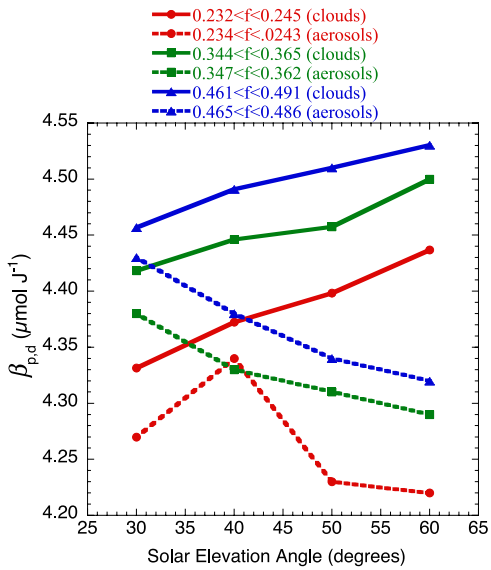

Figure 6. The relation between the quanta-to-energy ratio for diffuse irradiation of PAR ($\beta_{p,d}$) and solar elevation angle (SEA) for various observed values of f (diffuse fraction of global PAR) where $f = f_{p,d}$. Common line colors indicate similar ranges of $f_{p,d}$. Solid lines represent cloud-dominated scattering (this study), whereas broken lines represent data for fine aerosol-dominated scattering reported by *McCartney* [1978].

attributed to differences in the radiation scattering processes by which clouds (spectrally neutral scattering) and fine mode aerosols (greater scattering at shorter wavelengths) contribute to the diffuse PAR irradiance at the surface. Typically, the horizontal distribution of aerosols and aerosol properties is relatively homogeneous at the local scale, whereas for clouds and cloud properties it can be markedly inhomogeneous. In the case of a broken cloud field in a clean atmosphere, the spectral composition of the diffuse PAR on an unobstructed, horizontal surface results from the combination of two distinct scattering mechanisms: (1) selective (Rayleigh) scattering of PAR by the molecular atmosphere from all directions, and (2) nonselective scattering of PAR that passes through or is diffusely reflected by clouds.

[26] The diffuse PAR flux emanating from the cloud gaps is the product of Rayleigh scattering by the molecular atmosphere and thus exhibits a blue-sky spectrum [*Endler*, 1993], similar to the clear-sky case ($f'_{p,d} \approx 0.16$) in Figure 3. The diffuse PAR flux emanating from clouds is dominated by non-selective scattering or diffuse reflectance and thus exhibits an essentially white-light spectrum that differs little from the spectrum of the direct beam PAR. In contrast, scattering by fine mode aerosols is strongly wavelength dependent in the PAR spectral region. Moreover, broken cloud fields may cause substantially greater variability in the source geometry of the diffuse flux than would be observed under a cloudless but turbid atmosphere.

[27] For $f_{p,d}$ to remain constant as SEA declines (Figure 6), the contribution of scattered PAR from clouds and aerosols to the diffuse flux must decline. In the case of broken clouds, it is likely that such a decline in $f_{p,d}$ would be associated with a decrease in the cloud fraction (fraction of sky obscured by clouds) or a decrease in the optical thickness of the broken or uniform cloud layer. A decrease in the cloud fraction and/or cloud optical thickness decreases the contribution of diffuse "white" light to the total diffuse irradiance at the surface, thereby reducing the relative contribution of green-to-red wavelength radiation to the spectral composition of the diffuse PAR. This effect evidently counteracts and dominates the opposing effect of Rayleigh and fine mode aerosol scattering, which increases the relative contribution of green-to-red light to the diffuse PAR flux as SEA declines. The contrasting patterns evident in Figure 6 demonstrate that clouds and aerosols can affect the spectral composition of diffuse PAR in different ways. Because aerosol absorption may be enhanced as a result of multiple scattering by clouds and is wavelength dependent, additional research would be necessary to separate the effects of scattering by clouds and aerosols on $\beta_{p,d}$ in environments where both contribute significantly to the observed range of $f_{p,d}$. Experimental evidence reported by *Erlick et al.* [1998] suggests that the shape of the atmospheric spectral transmission curve in the PAR region is dominated by the effect of scattering by cloud drops unless the optical depth of aerosols begins to approach the optical depth of the cloud.

3.2.2. Daily Timescale

[28] For diffuse PAR at the daily timescale, the complex relation between $\beta_{p,d}$ and $f_{p,d}$ (Figure 5a) converges to a simple nonlinear relation (Figure 7). The convergence is attributable the dominant influence of the PAR received at high sun angles on the daily integral of PAR. The value of $\beta'_{p,d}$ increases non-linearly by 7% (from 4.24 to 4.54 μmol J^{-1}) as the daily atmospheric scattering (measured by $f'_{p,d}$) increases from a minimum value associated with clear sky conditions (~0.13) to the maximum potential value (1.0) associated with continuously overcast conditions (Figure 7). The relation is expressed well ($R^2 = 0.961$) by a single, saturating curve (Figure 7), defined as

$$\beta'_{p,d} = \frac{4.5886 \cdot f'_{p,d}}{0.010773 + f'_{p,d}} \quad (5)$$

To my knowledge, such a continuous relation between $f'_{p,d}$ and $\beta'_{p,d}$, which represents a diverse range of instantaneous and daily cloud conditions (including cloudless, overcast, and broken clouds), has not been previously reported in the research literature.

[29] The increase of $\beta'_{p,d}$ with cloudiness (as indicated by variation in $f'_{p,d}$ in Figure 7) has potentially significant implications for terrestrial photosynthesis. Results from a sensitivity analysis (performed with a model that accounts separately for the effects of diffuse and beam PAR on forest canopy photosynthesis) suggests that the observed spectral shift in diffuse PAR under conditions of moderate atmospheric scattering (e.g., broken clouds), may increase the daily gross photosynthesis of the shaded portion of a tropical forest canopy by up to 6% (D. Dye, unpublished manuscript, 2004). The increase in photosynthesis is attributable to the additional photons per unit energy in the diffuse PAR flux that are intercepted and absorbed by the shaded leaves. This phenomenon occurs in conjunction with, but is physically distinct from, the effect of efficient distribution of diffuse PAR throughout the leaf canopy that has been noted in previous studies [e.g., *Healey et al.*, 1998; *Roderick et al.*, 2001; *Gu et al.*, 2002; *Farquhar and Roderick*, 2003].

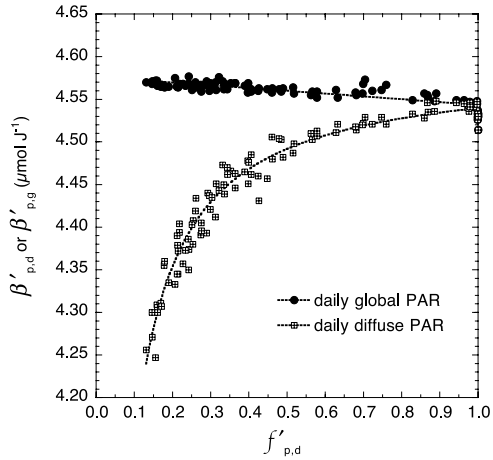

Figure 7. Relationship between the diffuse fraction of daily global irradiation of PAR ($f'_{p,d}$) and the quanta-to-energy ratio for daily diffuse irradiation of PAR ($\beta'_{p,d}$) and for daily global irradiation of PAR ($\beta'_{p,g}$). These results are based on spectral irradiance measurements made at the SGP site on 103 days during the period from March 1 to July 31, 2000.

[30] For global PAR, I employ least squares linear regression to quantify the relation between $\beta'_{p,g}$ and $f'_{p,d}$ (Figure 7). The regression equation ($R^2 = 0.689$) is

$$\beta'_{p,g} = 4.576 - 0.033144 \cdot f'_{p,d} \quad (6)$$

As $f'_{p,d}$ increases from 0.13 to 1.0, $\beta'_{p,g}$ exhibits a small (0.7%) decline from 4.57 to 4.54. Thus the spectral composition and quanta-to-energy ratio of global PAR ($\beta'_{p,g}$), while not strictly constant, is relatively insensitive to atmospheric scattering under the sky conditions observed in this study, in which clouds are the predominant scattering medium. Results from the present study suggest that $\beta'_{p,g} = 4.56$ μmol J^{-1}, which corresponds to moderate atmospheric scattering ($f'_{p,d} = 0.5$), may be confidently applied to global PAR data that represent diverse cloud conditions, with little or no error. Alternatively, when $f'_{p,d}$ is known, Equation 6 provides the potential for achieving a small, additional increment of accuracy in the energy-to-quanta unit conversion for global PAR. These results agree well with previous studies that suggest a fixed value of ~4.57 μmol J^{-1} could be adopted for $\beta'_{p,g}$ [*McCartney*, 1978; *Zhou and Xiang*, 1992; *Jacovides et al.*, 1997], regardless of whether the predominant scattering medium is clouds or fine mode aerosols.

[31] Variation in $\beta'_{p,d}$ and $\beta'_{p,g}$ not explained by Equations 5 and 6 may be attributable to variations in the spatial, geometrical, and/or optical properties of clouds and/or aerosols that influence the spectral composition of diffuse or global PAR, but are not adequately represented by $f'_{p,d}$. Scatter in the values of $\beta'_{p,d}$ and $\beta'_{p,g}$ under conditions of essentially 100% diffuse PAR ($\sim 0.97 \leq f_{p,d} \leq 1.0$) is substantially reduced in comparison to the 1-min timescale, and may be negligible for many general applications of Equations 5 and 6.

3.3. Generality of the Results

[32] The results described above are obtained from spectral irradiance measurements collected at a single, midlatitude site. At other locations around the globe, differences in one or more environmental factors may cause the relations between the diffuse fraction of global PAR and the quanta-to-energy ratio to deviate from those depicted in Figures 5 and 7. The key factors may include differences in surface elevation (clear-sky Rayleigh optical thickness), latitude (daily range of solar elevation angles), surface albedo (surface-atmosphere multiple scattering), and the abundance and physical properties of clouds and aerosols (three-dimensional scattering effects and spectral absorptivity). A quantitative evaluation of the significance of these factors *vis a vis* Equation 5 may be achieved in future research through an analysis of spectral irradiance data collected in multiple, diverse environments, and possibly through detailed, three-dimensional modeling of atmospheric spectral radiative transfer. In the meantime, general application of Equation 5 warrants caution.

4. Summary and Conclusions

[33] This study analyzed a time series data set of 1-min average measurements of spectral irradiance of PAR collected at the Southern Great Plains ARM site in Oklahoma, USA on 103 days in the period between March 1 and July 31 of 2000. The data represent a broad range of solar elevation angles (0.4 to 76.8 degrees) and a comprehensive range of magnitudes of atmospheric scattering (and associated sky conditions) as inferred from variation in the diffuse fraction of global PAR ($f_{p,d}$) at the 1-min timescale. The results indicate that the relative contribution of green-to-red (550–700 nm) light to the spectral composition of diffuse PAR increases as the diffuse fraction of daily global PAR ($f'_{p,d}$) increases from an effective minimum value (~0.13) associated with clear sky conditions to the maximum potential value (1.0) associated with overcast conditions (Figures 3 and 4). This spectral shift causes the quanta-to-energy ratio for daily diffuse PAR ($\beta'_{p,d}$) to increase by 7% (from 4.24 to 4.54 μmol J^{-1}) (Figure 7).

[34] Several recent studies have emphasized the importance of accounting for diffuse PAR in models of terrestrial photosynthesis and ecosystem-atmosphere carbon exchange [*Healey et al.*, 1998; *Roderick et al.*, 2001; *Gu et al.*, 2002; *Farquhar and Roderick*, 2003]. Currently, suitable data sets for PAR (particularly diffuse PAR) are rare in comparison to those for broadband solar irradiance. Consequently, meeting the PAR data requirements of detailed process models of photosynthesis and the terrestrial carbon cycle may often depend on the conversion of measured or estimated PAR data from energy units (irradiance) to quantum units (photon flux density). The results from the present analysis suggest that maximum accuracy in such unit conversion requires accounting for the changes in the spectral composition of diffuse PAR associated with variation in the magnitude of atmospheric scattering. Failure to account for this phenomenon may cause errors of up to 7% in the resulting quantum values when clouds are the primary scattering medium. When $f'_{p,d}$ is known, Equation 5 provides a practical means for estimating an appropriate value of $\beta'_{p,d}$ for the observed cloud conditions. Incorporating this relation into ecosystem process models that require conversion of diffuse PAR data from energy units to quantum units may contribute toward improved accuracy in simulations of vegetation canopy photosynthesis. A quantitative evaluation of the robustness of Equation 5 for sites with contrasting environmental conditions (e.g., surface elevation, latitude, surface albedo, and the abundance and physical properties of clouds and aerosols) is a desirable objective for future research.

Appendix A: Calculation of Energy and Photon Quantities

[35] Irradiation ($R'_{i,n}$, J m^{-2}) is calculated from the measured spectral irradiance (W m^{-2} nm^{-1}) as

$$R'_{i,n} = R_{i,n} \cdot \Delta_i \cdot \Delta_t \quad (A1)$$

where Δ_i is the spectral interval (nm) associated with RSS channel i, and Δ_t is the measurement interval (60 s). In the absence of specific information on the bandpass sensitivities of the individual RSS channels, I approximate Δ_i as

$$\Delta_i = \left(\frac{\lambda(i) + \lambda(i+1)}{2}\right) - \left(\frac{\lambda(i) + \lambda(i-1)}{2}\right) \quad (A2)$$

where $\lambda(i)$ is the nominal, central wavelength of the interval. The value of Δ_i increases nonlinearly from

0.24 nm to 1.11 nm as $\lambda(i)$ increases across the PAR band. For each value of $R'_{i,n}$, I calculate the equivalent photon exposure $Q'_{i,n}$ (μmol m^{-2}) as

$$Q'_{i,n} = \beta_{\lambda(i)} \cdot R'_{i,n} \tag{A3}$$

where $\beta_{\lambda(i)}$ is the quanta-to-energy ratio (μmol J^{-1}) for monochromatic radiation of wavelength $\lambda(i)$, and $\lambda(i)$ is the central wavelength of the spectral interval for RSS channel i. I calculate $\beta_{\lambda(i)}$ by the equation

$$\beta_{\lambda(i)} = \left(M \cdot E_{\lambda(i)}\right)^{-1} \tag{A4}$$

where M is a mole (Avogadro's number, = 6.023×10^{23}) of photons, and $E_{\lambda(i)}$ is the energy (joules) of single photon of radiation with wavelength $\lambda(i)$. On the basis of quantum law, the energy is determined by

$$E_{\lambda(i)} = hc/\lambda(i) \tag{A5}$$

where $\lambda(i)$ has units of meters, h is Planck's constant (6.63×10^{-34} J s), and c is the speed of light (3.0×10^8 m s^{-1}). Strictly, Equations A4 and A5 are accurate only for monochromatic radiation; for a broad spectral interval such as the PAR band ($\Delta_p = 700-400 = 300$), the assumption that $\beta_{\lambda(i)}$ is representative of the interval would introduce large errors and is untenable. Because this assumption is adopted only for contiguous, narrow spectral intervals ($0.24 \leq \Delta_i \leq 1.11$) for integration across the PAR band, the associated errors in the integrated PAR values become negligible.

[36] With the narrow-band results from Equations A1 and A3, for each measurement period t, I calculate the irradiation of PAR ($R'_{p,n}$, J m^{-2}) as

$$R'_{p,n,t} = \sum_{i=190}^{762} R'_{i,n,t} \tag{A6}$$

and the photon exposure of PAR ($Q'_{p,n}$, μmol m^{-2}) as

$$Q'_{p,n,t} = \sum_{i=190}^{762} Q'_{i,n,t} \tag{A7}$$

The daily total radiant exposure ($R''_{p,n}$, MJ m^{-2}) and the daily total photon exposure ($Q''_{p,n}$, mol m^{-2}) are determined by summing the results from Equations A6 and A7, respectively, for each daily time series of measurements.

Notation

PAR	photosynthetically active radiation, 400–700 nm.
Q_p	photosynthetic photon flux density, μmol m^{-2} s^{-1}.
R_p	irradiance of PAR, W m^{-2}.
R_s	irradiance of broadband solar (shortwave) radiation, W m^{-2}.
p	PAR.
s	broadband solar (shortwave) radiation.
$\beta^*_{p,n}$	quanta-to-energy ratio for PAR at an arbitrary timescale, μmol J^{-1}.
n	g, d, or b.
g	global.
d	diffuse.
b	direct beam.
$R_{d,p}$	diffuse irradiance of PAR, W m^{-2}.
$R_{d,s}$	diffuse irradiance of broadband solar (shortwave) radiation, W m^{-2}.
RSS	Rotating Shadowband Spectroradiometer.
SGP	Southern Great Plains.
ARM	Atmospheric Radiation Measurement (Program).
SEA	solar elevation angle (degrees).
$R_{i,n}$	spectral irradiance, W m^{-2} nm^{-1}.
i	spectral channel number of RSS instrument ($1 \leq i \leq 1016$).
λ	wavelength, nm.
$\beta_{p,n}$	quanta-to-energy ratio for PAR at 1-minute timescale, μmol J^{-1}.
$\beta'_{p,n}$	quanta-to-energy ratio for PAR at daily timescale, μmol J^{-1}.
$R'_{p,n}$	irradiation of PAR for 1-min interval, J m^{-2}.
$R''_{p,n}$	daily total irradiation of PAR, MJ m^{-2}.
$Q'_{p,n}$	photon exposure of PAR for 1-min interval, μmol m^{-2}.
$Q''_{p,n}$	daily total photon exposure of PAR, mol m^{-2}.
NDPSI	Normalized Difference PAR Spectral Index (dimensionless).
$NDPSI'_{E,n}$	NDPSI for energy at daily timescale (dimensionless).
$NDPSI'_{Q,n}$	NDPSI for quanta at daily timescale (dimensionless).
puv	400–550 nm spectral wave band.
pir	550–700 nm spectral wave band.
$f_{p,d}$	diffuse fraction of global irradiation of PAR at 1-min timescale (dimensionless).
$f'_{p,d}$	diffuse fraction of global irradiation of PAR at daily timescale (dimensionless)
Δ_i	spectral interval (nm) associated with RSS channel i.
Δ_t	time interval of RSS spectral irradiance measurement (60 s).
$Q'_{i,n}$	daily photon exposure of PAR for RSS channel i, μmol m^{-2}.
$\beta_{\lambda(i)}$	quanta-to-energy ratio (μmol J^{-1}) for monochromatic radiation of wavelength $\lambda(i)$.
$\lambda(i)$	central wavelength of spectral interval for RSS channel i.
$R'_{i,n}$	irradiation (J m^{-2}) for 1-min interval and for monochromatic radiation of wavelength $\lambda(i)$.
M	1 mole (Avogadro's number, = 6.023×10^{23}) of photons.
$E_{\lambda(i)}$	energy (joules) of a single photon of radiation with wavelength $\lambda(i)$ (meters).
h	Planck's constant, 6.63×10^{-34} J s.
c	speed of light, 3.0×10^8 m s^{-1}.
t	index number of a sequential 1-min measurement period.

[37] **Acknowledgments.** I thank Lee Harrison and colleagues (Atmospheric Sciences Research Center, SUNY Albany) for providing the RSS spectral irradiance data, and Tom Eck (UMBC-GEST and NASA-GSFC) for his insightful and constructive comments on the initial manuscript.

ARM data are made available through the U.S. Department of Energy as part of the Atmospheric Radiation Measurement Program.

References

Allen, L. H., Jr., D. W. Stewart, and E. R. Lemon (1974), Photosynthesis in plant canopies: Effect of light response curves and radiation source geometry, *Photosynthetica*, *8*, 184–207.

Bishop, J. K. B., and W. B. Rossow (1991), Spatial and temporal variability of global surface solar irradiance, *J. Geophys. Res.*, *96*, 16,839–16,858.

Brine, D. T., and M. Iqbal (1983), Diffuse and global solar spectral irradiance under cloudless skies, *Sol. Energ.*, *30*, 447–453.

Data Assimilation Office (2003), *File Specification for GEOS-DAS Gridded Output Version 5.2*, Goddard Lab. for Atmos., Goddard Space Flight Cent., Greenbelt, Md.

Diermendjian, D., and Z. Sekera (1954), Global radiation resulting from multiple scattering in a Rayleigh atmosphere, *Tellus*, *6*, 382–398.

Dye, D. G., and R. Shibasaki (1995), Intercomparison of global PAR data sets, *Geophys. Res. Lett.*, *22*, 2013–2016.

Eck, T., et al. (2003), Variability of biomass burning aerosol optical characteristics in southern Africa during the SAFARI 2000 dry season campaign and a comparison of single scattering albedo estimates from radiometric measurements, *J. Geophys. Res.*, *108*(D13), 8477, doi:10.1029/2002JD002321.

Endler, J. (1993), The color of light in forests and its implications, *Ecol. Monogr.*, *63*, 1–27.

Erlick, C., J. E. Frederick, V. K. Saxena, and B. N. Wenny (1998), Atmospheric transmission in the ultraviolet and visible: Aerosols in cloudy atmospheres, *J. Geophys. Res.*, *103*(D24), 31,541–31,556.

Farquhar, G. D., and M. L. Roderick (2003), Pinatubo, diffuse light, and the carbon cycle, *Science*, *299*, 1997–1998.

Frouin, R., D. W. Lingner, C. Gautier, K. Baker, and R. C. Smith (1989), A simple analytical formula to compute clear sky total and photosynthetically available solar irradiance at the ocean surface, *J. Geophys. Res.*, *94*, 9731–9742.

Gates, D. M. (1966), Spectral distribution of solar radiation at the Earth's surface, *Science*, *151*, 523–529.

Gu, L., D. Baldocchi, S. Verma, T. Black, T. Vesala, E. Falge, and P. Dowty (2002), Advantages of diffuse radiation for terrestrial ecosystem productivity, *J. Geophys. Res.*, *107*(D6), 4050, doi:10.1029/2001JD001242.

Hall, D. O., and K. K. Rao (1994), *Photosynthesis*, 5th ed., 211 pp., Cambridge Univ. Press, New York.

Harrison, L., M. Beauharnois, J. Berndt, P. Kiedron, J. Michalsk, and Q. Min (1999), The rotating shadowband spectroradiometer (RSS) at SGP, *Geophys. Res. Lett.*, *26*, 1715–1718.

Healey, K. D., K. G. Rickert, G. L. Hammer, and M. P. Bange (1998), Radiation use efficiency increases when the diffuse component of incident radiation is enhanced under shade, *Aust. J. Agric. Res.*, *49*, 665–672.

Hinds, W. C. (1999), *Aerosol Technology: Properties, Behavior, and Measurement of Airborne Particles*, 483 pp., John Wiley, Hoboken, N. J.

Iziomon, M. G., and U. Lohmann (2003), Characteristics, impacts and direct radiative forcing of aerosols at the ARM Southern Great Plains Central Facility, *Atmos. Chem. Phys. Discuss.*, *3*, 2353–2391.

Jacovides, C. P., F. Timbios, D. N. Asimakopoulos, and M. D. Steven (1997), Urban aerosol and clear skies spectra for global and diffuse photosynthetically active radiation, *Agric. For. Meteorol.*, *87*, 91–104.

McCartney, H. A. (1978), Spectral distribution of solar radiation, II: Global and diffuse, *Q. J. R. Meteorol. Soc.*, *104*, 911–926.

McCree, K. J. (1972), Test of current definitions of photosynthetically active radiation against leaf photosynthesis data, *Agric. Meteorol.*, *10*, 443–453.

McCree, K. J. (1976), A comparison of experimental and theoretical spectra for photosynthetically active radiation at various atmospheric turbidities, *Agric. Meteorol.*, *16*, 405–412.

Medlyn, B., D. Barrett, J. Landsberg, P. Sands, and R. Clement (2003), Conversion of canopy intercepted radiation to photosynthate: Review of modelling approaches for regional scales, *Funct. Plant Biol.*, *30*, 153–169.

Michalsky, J. J., J. A. Schlemmer, W. E. Berkheiser, J. L. Berndt, L. C. Harrison, N. S. Laulainen, N. R. Larson, and J. C. Barnard (2001), Multiyear measurements of aerosol optical depth in the Atmospheric Radiation Measurement and Quantitative Links programs, *J. Geophys. Res*, *106*(D11), 12,099–12,107.

Pinker, R. T., and I. Laszlo (1992), Global distribution of photosynthetically active radiation as observed from satellites, *J. Clim.*, *5*, 56–65.

Roderick, M. L., G. D. Farquhar, S. L. Berry, and I. R. Noble (2001), On the direct effect of clouds and atmospheric particles on the productivity and structure of vegetation, *Oecologia*, *129*, 21–30.

Ross, J., and M. Sulev (2000), Sources of errors in measurements of PAR, *Agric. For. Meteorol.*, *100*, 103–125.

Rutan, D. A., F. G. Rose, N. M. Smith, and T. P. Charlock (2001), Validation data set for CERES surface and atmospheric radiation budget (SARB), *WCRP/GEWEX Newslett.*, *11*(1), 11–12.

Salby, M. L. (1996), *Fundamentals of Atmospheric Physics*, 627 pp., Academic, San Diego, Calif.

Zhou, Y., and Y. Xiang (1992), Measurement and empirical estimate of photosynthetically active radiation, *J. Chin. Geogr.*, *3*, 55–71.

D. G. Dye, Ecosystem Change Research Program, JAMSTEC-FRSGC, 3173-25 Showa-machi, Kanazawa-ku, Yokohama, Kanagawa-ken, 236-0001, Japan. (dye@jamstec.go.jp)